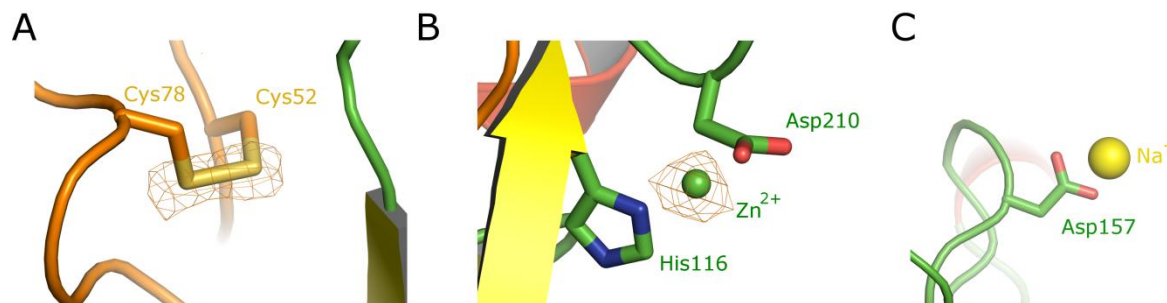
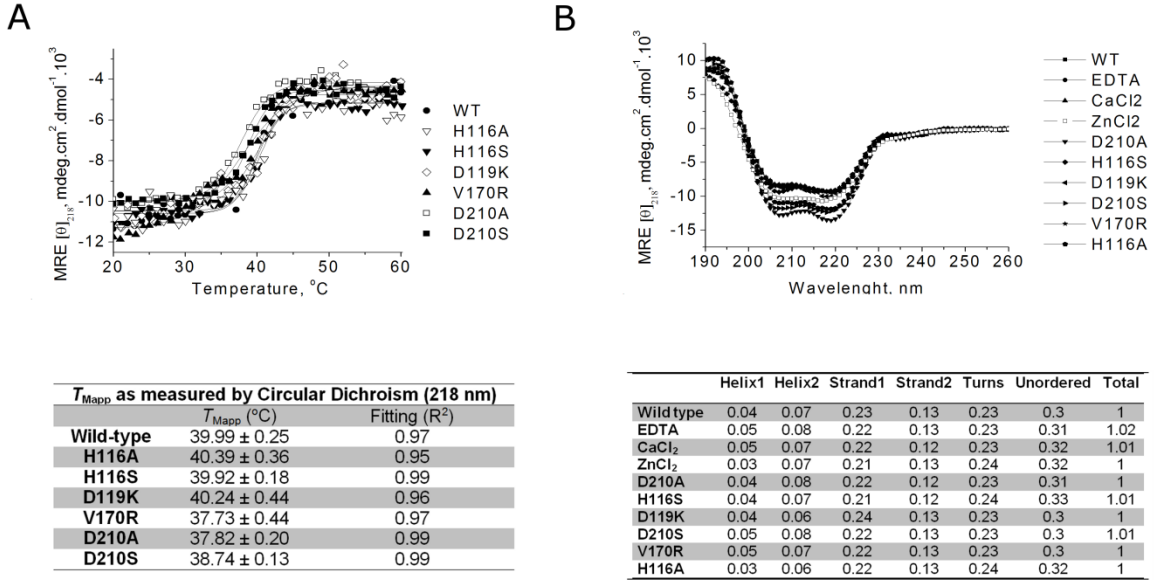


**Figure S1**



*Figure S1. Identification of binding metals in MpNEP2 crystal structure.* X-ray diffraction data set collected at a wavelength of 1.608 Å presented clear peaks in the Fourier anomalous map contoured at 3σ (orange mesh representation). Due to size, shape and chemical environment, they were readily identified as metal ions and, based on the protein purification protocol and crystallization condition, possible candidates were sodium, zinc and cobalt. The contribution of zinc to the  $f'$  component of the atomic scattering factor at the correspondent energy is 0.73 electrons (as calculated by the software CROSSEC (1), which is very similar to the contribution of sulfur (0.60 electrons). As the wavelength used corresponded to the absorption edge of the K-shell of cobalt, the same, if present in the structure, should contribute with 3.9 electrons to the dispersive term of the scattering factor. We used the peaks heights in the Fourier anomalous map at the disulfide bridge as a standard (A) to determine the nature of the metals present in our structure. Only one of the two positions initially identified as metals had similar contour levels to the sulfur peaks and therefore was interpreted as zinc (B). At the site where the other metal should be, no peaks in the anomalous map were found. According to this observation and to the chemical environment, sodium was modeled (C).

**Figure S2**



*Figure S2. Thermal stability and conservation of the folding features across the MpNEP2 mutants. (A) The point mutants used in this manuscript were tested for folding stability as inferred from the  $T_{Mapp}$  calculated from MRE  $[\theta]_{218 \text{ nm}}$ , at a range of temperatures (see table below for the values). (B) Far-UV CD spectrum measurement (190-260 nm) of MpNEP2 wild-type (incubated with EDTA or CaCl<sub>2</sub>/ZnCl<sub>2</sub>) and mutants. Secondary structure was estimated on DICHROWEB interface (2) using CDSSTR method (2) and the Reference Protein Set #4 (table below).*

**Figure S3**

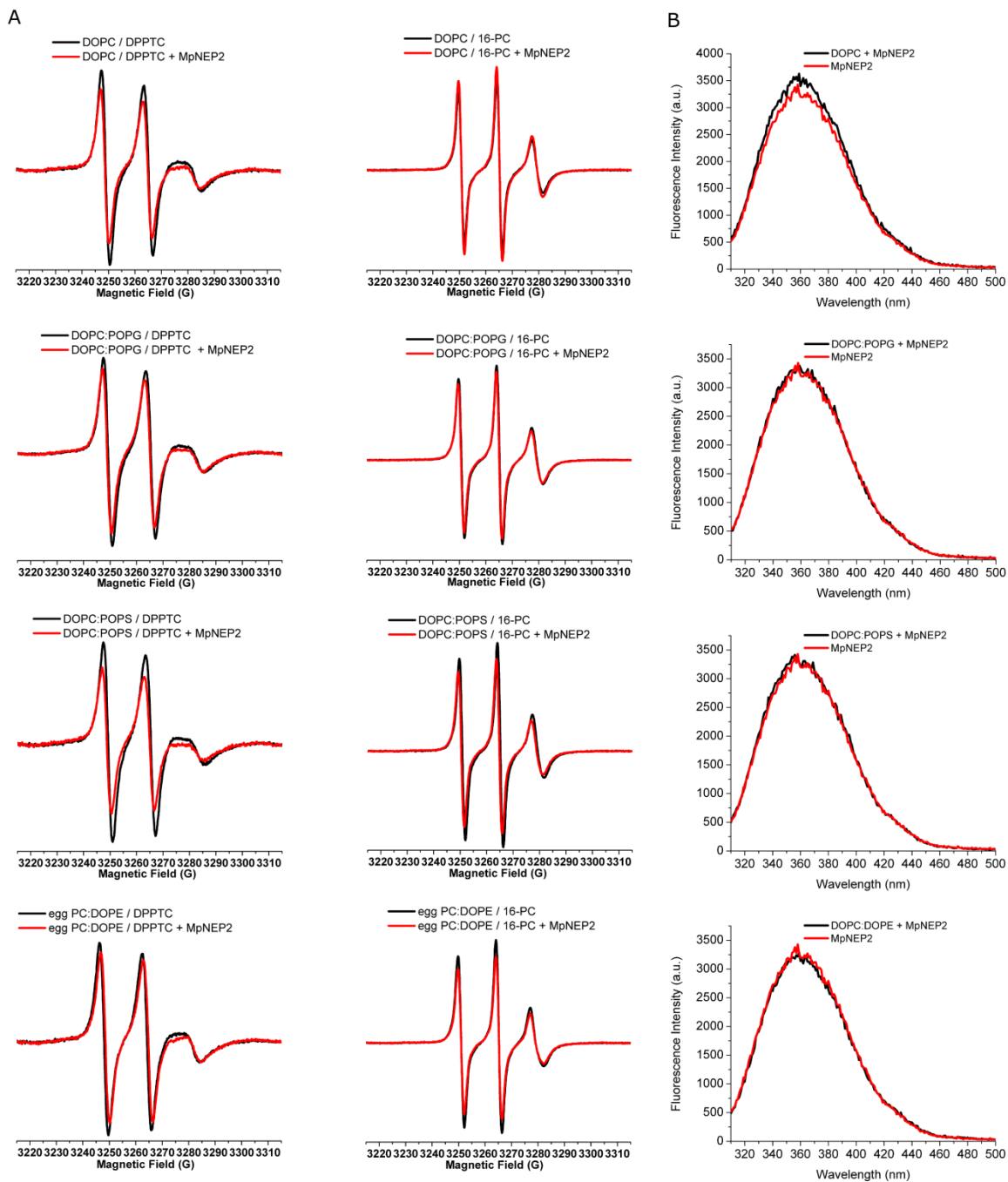


*Figure S3. Electron paramagnetic resonance and intrinsic fluorescence assays. (A) The EPR spectra of the headgroup spin probe (DPPTC – on the left) or the acyl chain-labeled (16-PC – on the right) incorporated into DOPC, DOPC:POPG (2:1 molar ratio), DOPC:POPS (2:1 molar*

ratio) and egg PC:DOPE (2:1 molar ratio) LUVs in the presence or absence of MpNEP2 showed no changes in their profile at a 1:100 protein:LUV ratio (mol:mol). (B) The intrinsic fluorescence measurements of 2  $\mu$ M MpNEP2 indicated no significant perturbation in the tryptophan emission spectra after addition of a 100-fold molar excess of the DOPC, DOPC:POPG, DOPC:POPS, or DOPC:DOPE non-labeled LUVs.

**Figure S4**

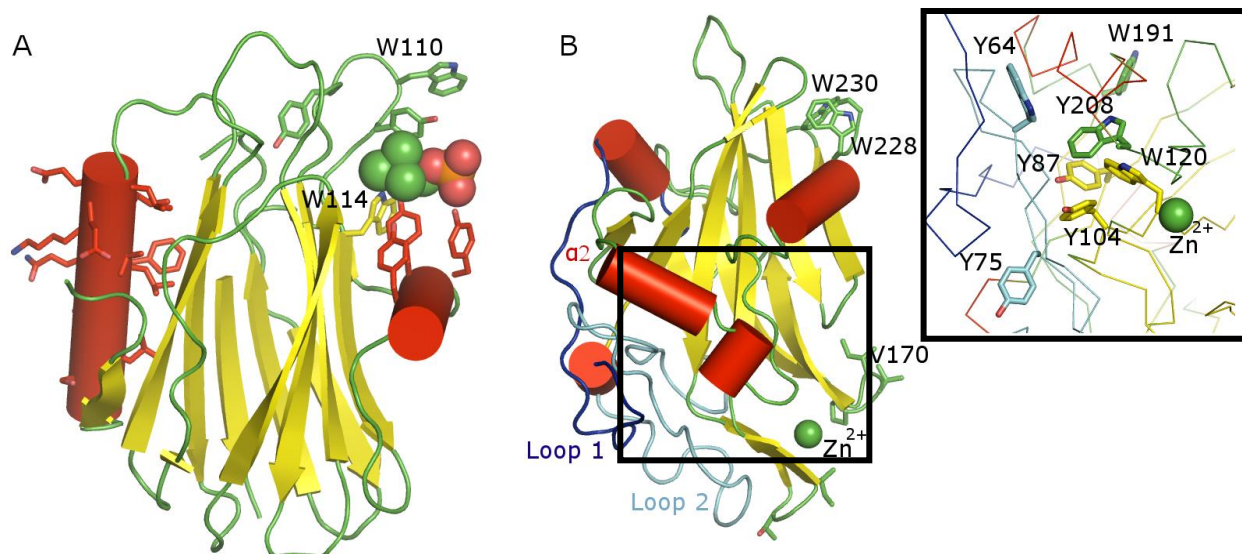


Figure S4. Comparison between the actinoporin sticholysin II and MpNEP2 structures. Sticholysin II (A) and MpNEP2 (B) structures represented as cartoon and colored according to secondary structure ( $\alpha$ -helices in red,  $\beta$ -strands in yellow and loops in green, dark blue and cyan). Sticholysin was co-crystallized with phosphocoline (represented as spheres) (3). Inset figure on the right corner reveals MpNEP2 aromatic residues from the  $\beta$ -sheet core involved on stabilizing loop 2 and  $\alpha$ -helix 2 closely packed to the protein body. Membrane binding could potentially induce the displacement of this loop and helix to create a lipophilic surface.

1. Waasmaier, D., and Kirfel, A. (1995) New Analytical Scattering Factor Functions for Free Atoms and Ions, *Acta Cryst. A* 51.
2. Whitmore, L., and Wallace, B.A. (2008) Protein Secondary Structure Analyses from Circular Dichroism Spectroscopy: Methods and Reference Databases, *Biopolymers* 89, 392-400.

3. Mancheño, J.M., Martín-Benito, J., Martínez-Ripoll, M., Gavilanes, J.G, and Hermoso, J.A. (2003) Crystal and Electron Microscopy Structures of Sticholysin II Actinoporin Reveal Insights into the Mechanism of Membrane Pore Formation, *Structure 11*, 1319-1328.